



Dalton
Transactions

**Expanding the Synthetic Toolbox to Access Pristine and
Rare-Earth-Doped BaFBr Nanocrystals**

Journal:	<i>Dalton Transactions</i>
Manuscript ID	DT-ART-08-2021-002694.R1
Article Type:	Paper
Date Submitted by the Author:	22-Sep-2021
Complete List of Authors:	Dhanapala, B. Dulani; Wayne State University, Chemistry Munasinghe, Hashini; Wayne State University, Chemistry Dissanayake, K.; Wayne State University, Chemistry Suescun, Leopoldo; Universidad de la República, Facultad de Química Rabuffetti, Federico; Wayne State University, Chemistry

SCHOLARONE™
Manuscripts

ARTICLE

Expanding the Synthetic Toolbox to Access Pristine and Rare-Earth-Doped BaFBr Nanocrystals

Received 00th January 20xx,
Accepted 00th January 20xx

B. Dulani Dhanapala,^a Hashini N. Munasinghe,^a K. Tauni Dissanayake,^a Leopoldo Suescun,^b and Federico A. Rabuffetti^{a,†}

DOI: 10.1039/x0xx00000x

A new synthetic route to pristine and rare-earth-doped BaFBr nanocrystals is described. Central to this route is an organic–inorganic hybrid precursor of formula $\text{Ba}_5(\text{CF}_2\text{BrCOO})_{10}(\text{H}_2\text{O})_7$ that serves as a dual-halogen source. Thermolysis of this precursor in a mixture of high-boiling point organic solvents yields spherical BaFBr nanocrystals (≈ 20 nm in diameter). Yb:Er:BaFBr nanocuboids (≈ 26 nm in length) are obtained following the same route. Rare-earth-doped nanocrystals display NIR-to-visible photon upconversion under 980 nm excitation. The temperature-dependence of the green emission from Er^{3+} may be exploited for optical temperature sensing between 150 and 450 K, achieving a sensitivity of $1.1 \times 10^{-2} \text{ K}^{-1}$ and a mean calculated temperature of 300.9 ± 1.5 K at 300 K. The synthetic route presented herein not only enables access to an unexplored upconverting material, but also and more importantly, creates the opportunity to develop solution-processable photostimulable phosphors based on BaFBr.

Introduction

Rare-earth-doped BaFX (X = Cl, Br, I) constitute technologically relevant materials in the field of photostimulable phosphors used in medical X-ray imaging.^{1–3} BaFBr in particular is the archetypical platform in which iso- and aliovalent substitutions with alkaline-earth metals,^{4–6} halogens,^{3, 6, 7} and rare-earths^{6, 8} are performed to tune luminescence response. Polycrystalline rare-earth-doped BaFBr bulk phosphors may be synthesized using high-temperature solid-state reaction.^{4, 5, 7, 9, 10} This route relies on barium and ammonium halides as fluorine and bromine sources. Over the past ten years, however, alternative synthetic approaches have been developed with the aim of achieving control over the morphology of the phosphor grains. These developments have been motivated by the realization that phosphor morphology directly impacts optical data storage performance (e.g., image quality and spatial resolution).¹¹ As a result, a variety of routes to nano- and submicron-sized rare-earth-doped BaFBr crystals have been described in the literature. These routes include oil-in-water microemulsions,^{12, 13} coprecipitation,^{14, 15} mechanochemical,^{6, 16} and ionic liquid-assisted synthesis.¹⁷ Colloidal synthesis in high-boiling point organic solvents is a remarkable absence in this toolbox, despite its potential to afford size- and shape-controlled nano- and submicrocrystals

that can be solution-processed into functional form factors (i.e., imaging plates).

Recently, our group reported metal heterohaloacetates as a new family of precursors for the solid-state and solution phase synthesis of mixed halides.¹⁸ These precursors are synthesized starting from a metal salt and commercially available heterohaloacetic acids and provide a convenient way to prepare pristine and doped fluorohalide nanocrystals via colloidal routes. In this article we further develop that chemistry to expand the synthetic toolkit enabling access to rare-earth-doped BaFBr nanocrystals. $\text{Ba}_5(\text{CF}_2\text{BrCOO})_{10}(\text{H}_2\text{O})_7$ is used as a precursor to pristine and doped BaFBr nanocrystals. Its synthesis and crystal structure are described and its reactivity is investigated in the solid-state and in solution. BaFBr and Yb:Er:BaFBr nanocrystals are obtained upon hot injection of $\text{Ba}_5(\text{CF}_2\text{BrCOO})_{10}(\text{H}_2\text{O})_7$ into a mixture of oleic acid, 1-octadecene, and trioctylphosphine. The resulting nanocrystals are characterized in regards to their phase purity, morphology, doping levels, and luminescence. A new ytterbium-sensitized NIR-to-visible upconverting material suitable for optical temperature sensing is thus realized. Findings presented herein further highlight the utility of metal heterohaloacetates as dual-halogen precursors for the colloidal synthesis of mixed-halide optical materials.

Experimental

Synthesis. All syntheses were conducted under nitrogen atmosphere using standard Schlenk techniques. Yb_2O_3 (99.9%), Er_2O_3 (99.99%), BaCO_3 (99.98%), anhydrous CF_3COOH (99%), oleic acid (90%), 1-octadecene (90%), and trioctylphosphine (97%) were purchased from Sigma-Aldrich and used as received. CF_2BrCOOH was purchased from SynQuest Laboratories and

^a Department of Chemistry, Wayne State University, Detroit, MI 48202, USA.

^b Crysmat-Lab/DETEMA, Facultad de Química, Universidad de la República, Montevideo 11800, Uruguay.

† Corresponding author. Email: far@chem.wayne.edu

Electronic Supplementary Information (ESI) available: (1) structural determination and crystal data of $\text{Ba}_5(\text{CF}_2\text{BrCOO})_{10}(\text{H}_2\text{O})_7$, and (2) additional analyses of the chemical composition, morphology, and luminescence of Yb:Er:BaFBr nanocrystals. See DOI: 10.1039/x0xx00000x

stored in a nitrogen-filled glovebox (oxygen and water levels below 1 ppm).

Synthesis of $\text{Ba}_5(\text{CF}_2\text{BrCOO})_{10}(\text{H}_2\text{O})_7$. $\text{Ba}_5(\text{CF}_2\text{BrCOO})_{10}(\text{H}_2\text{O})_7$ was synthesized via solvent evaporation.¹⁸ First, 2 mmol of CF_2BrCOOH were weighed inside a glovebox and transferred to a 50 mL two-neck round-bottom flask containing 6 mL of double-distilled water. Next, 1 mmol of BaCO_3 was added to this solution. The flask was immersed in a sand bath and heated at 60 °C for 12 h until a colorless, transparent solution was obtained; magnetic stirring was employed to aid in the dissolution of BaCO_3 . Finally, solvent evaporation was conducted at 65 °C for 48 h under a constant flow of nitrogen (200 mL min^{-1}). The resulting polycrystalline solid, from which single crystals were recovered for structural analysis, was stored under a static nitrogen atmosphere.

Synthesis of BaFBr Nanocrystals. Nanocrystals were synthesized via a modified hot injection method.¹⁸ First, 1 mL of oleic acid and 1 mL of 1-octadecene were added to a 50 mL two-neck round-bottom flask containing 1 mmol of $\text{Ba}_5(\text{CF}_2\text{BrCOO})_{10}(\text{H}_2\text{O})_7$ (flask A). Next, 3 mL of oleic acid and 3 mL of 1-octadecene were added to a 100 mL flask (flask B). Both flasks were immersed in sand baths and heated to 115 °C under vacuum and vigorous magnetic stirring. After 45 min at 115 °C, the atmosphere of flask B was switched to nitrogen, a needle thermocouple was placed inside the flask in direct contact with the solution, and 4 mL of trioctylphosphine were quickly injected. Next, the temperature of flask B was increased to 300 °C and then the solution in flask A was swiftly injected. The reaction proceeded for 90 min at 300 °C. The flask was then removed from the sand bath and quenched to room temperature using a stream of air, yielding a turbid solution. BaFBr nanocrystals were recovered using a work-up procedure described elsewhere.¹⁸

Synthesis of Yb:Er:BaFBr Nanocrystals. Five Yb:Er:BaFBr samples were prepared, each with a total metal content of 1 mmol. Nominal total rare-earth concentrations (Yb:Er:Ba molar ratios) of 0.50 mol. % (0.0045:0.0005:0.9950), 1.5 mol. % (0.0135:0.0015:0.9850), 3.0 mol. % (0.0270:0.0030:0.9700), 4.5 mol. % (0.0405:0.0045:0.9550), and 6.0 mol. % (0.0540:0.0060:0.9400) were targeted. The nominal erbium concentration was fixed at 10.0% of the total rare-earth content (Yb:Er molar ratio equal to 9). Polycrystalline precursors to Yb:Er:BaFBr nanocrystals were synthesized by dissolving stoichiometric amounts of Yb_2O_3 , Er_2O_3 , and BaCO_3 in a solution of 1 mL of CF_3COOH and 5 mL of H_2O . A colorless, transparent solution was obtained after heating at 65 °C for 12 h. Then, 2 mmol of CF_2BrCOOH were weighed inside a glovebox and quickly added to this solution; magnetic stirring aided in the dissolution of CF_2BrCOOH . Upon complete dissolution, solvent evaporation was conducted under the same conditions described above to yield polycrystalline solids. Once in hand, these precursors were decomposed to Yb:Er:BaFBr nanocrystals using a hot injection approach similar to that outlined for BaFBr. The only differences were that (1) precursors were dissolved in a mixture consisting of 1 mL of oleic acid and 1 mL of 1-octadecene and injected into a flask containing a mixture of

oleic acid (1 mL), 1-octadecene (1 mL) and trioctylphosphine (8 mL), and (2) the reaction proceeded for 20 min at 300 °C.

Single-Crystal X-ray Diffraction (SCXRD). SCXRD analysis was carried out using a Bruker X8 Apex single-crystal diffractometer. $\text{Ba}_5(\text{CF}_2\text{BrCOO})_{10}(\text{H}_2\text{O})_7$ crystals were mixed with Paratone oil under nitrogen atmosphere prior to mounting. A colourless crystal with approximate dimensions 0.301 × 0.444 × 0.574 mm was selected for structure determination and mounted on a microloop. X-ray diffraction intensities were measured at 100 K using Mo $K\alpha$ radiation ($\lambda = 0.71073 \text{ \AA}$). Frames were integrated using Bruker's SAINT software. Experimental data were corrected for Lorentz, polarization, and absorption effects; for the latter, the multiscan method was employed using Bruker's SADABS software.¹⁹ The crystal structure was solved using (1) a dual-space approach as implemented in SHELXT,²⁰ and (2) difference Fourier (ΔF) maps as embedded in SHELXL-2018/1²¹ running under ShelXle.²² The structure was visualized using VESTA.²³ Hydrogen atoms belonging to water molecules were not clearly visible in ΔF maps. They were not included in the final structural model because unambiguous determination of their positions using geometrical restrictions was not possible. Full details on the data collection, structure refinement, and structural data are given in the ESI (Tables S1–S4 and Figure S1). Crystal data were deposited in the Cambridge Crystallographic Data Centre with number 1961033.

Powder X-ray Diffraction (PXRD). PXRD patterns were collected at room temperature using a Bruker D2 Phaser operated at 30 kV and 10 mA. Cu $K\alpha$ radiation ($\lambda = 1.5418 \text{ \AA}$) was employed. A nickel filter was used to remove Cu $K\beta$. A step size of 0.025° and a step time of 0.5 s were used to collect diffractograms in the 10–60° 2θ range.

Rietveld Analysis. Rietveld analysis^{24, 25} of PXRD patterns was performed using the General Structural System (GSAS) with the graphical user interface (EXPGUI) software.^{26, 27} The crystal structures of BaFBr and Yb:Er:BaFBr were refined using the tetragonal $P4/nmm$ space group. The following parameters were refined: (1) scale factor; (2) background, which was modeled using a shifted Chebyshev polynomial function; (3) peak shape, which was modeled using a modified Thompson–Cox–Hasting pseudo-Voigt function;²⁸ (4) lattice constants (a and c); (5) fractional atomic coordinates of the metal (z_{Ba}) and bromine (z_{Br}) atoms; and (6) an isotropic displacement parameter for all atoms (U^{iso}). In the case of Yb:Er:BaFBr nanocrystals, the occupancy of the metal site (M) was fixed according to the Yb:Er:Ba ratio obtained from elemental analysis. Visual inspection of the difference curves and R_{wp} residual values were used to assess the quality of the refinements.

Thermal Analysis (TGA/DTA). Thermogravimetric (TGA) and differential thermal analyses (DTA) were conducted using an SDT2960 TGA–DTA analyzer (TA instruments). ≈ 10 mg of the precursor were placed in an alumina crucible, held at 35 °C for 30 min under a flow of argon (100 mL min^{-1}), and ramped to 600 °C at a rate of 10 °C min^{-1} .

Transmission Electron Microscopy Imaging (TEM). TEM images were obtained using a Thermo Scientific Talos F200X G2 S/TEM or a JEOL JEM2010F (JEOL Ltd.). 200 kV was used as the

accelerating voltage. A small aliquot of the native solution containing Yb:Er:BaFBr nanocrystals was diluted with toluene and drop-casted onto a 200 mesh Cu grid coated with a Lacey carbon film (Ted Pella Inc.). Size distribution histograms were obtained after analyzing 250–300 nanocrystals.

Inductively Coupled Plasma Mass Spectrometry (ICP–MS).

Elemental analyses of metals in Yb:Er:BaFBr nanocrystals were carried out using a 7700 Series ICP–MS (Agilent Technologies). $\approx 3\text{--}4$ mg of sample were dissolved in 20 mL of aqua regia at 65 °C. Ytterbium ($1000\ \mu\text{g mL}^{-1}$, High Purity Standards), erbium ($998\ \mu\text{g mL}^{-1}$, Fluka), and barium ($1000\ \mu\text{g mL}^{-1}$, High Purity Standards) in 2% HNO_3 were used as standards.

Spectrofluorometry. Spectrofluorometric analyses were conducted using a Fluorolog 3–222 fluorometer (Horiba Scientific). A MDL–N–980 (Opto Engine, LLC) continuous-wave 980 nm laser and an R928 photomultiplier tube were used as source and detector, respectively. Room temperature emission spectra were collected for all Yb:Er:BaFBr samples. Variable-temperature spectra were recorded for nanocrystals with a nominal total rare-earth concentration of 6.0 mol. %. In this case, the sample was loaded into a VPF–800 variable-temperature stage (Lake Shore Cryotronics) and degassed at 450 K for 2 h under vacuum (≈ 80 mTorr) prior to data collection. Temperature control was provided by a Lake Shore 335–3060 controller. Emission spectra were collected in the 150–450 K temperature range at 25 K intervals. A heating rate of $5\ \text{K min}^{-1}$ was employed. Samples were allowed to dwell for ≈ 10 min at the target temperature prior to spectra collection. All spectra

were recorded using a slit width of 2 nm and an excitation power density of $2.0\ \text{W cm}^{-2}$.

Results and Discussion

The crystal structure of $\text{Ba}_5(\text{CF}_2\text{BrCOO})_{10}(\text{H}_2\text{O})_7$ is shown in **Figures 1a** and **1b**. This extended inorganic hybrid²⁹ crystallizes in the $P2_12_12_1$ orthorhombic space group and is isostructural to its chlorodifluoro counterpart $\text{Ba}_5(\text{CF}_2\text{ClCOO})_{10}(\text{H}_2\text{O})_7$ first reported by our group.¹⁸ Barium atoms feature coordination numbers ranging from 8 to 11 and coordinating atoms include oxygen and fluorine from the carboxylate ligand and oxygen from water. $\text{Ba}(\text{O},\text{F})_n$ polyhedra share edges and faces to yield a three-dimensional framework displaying microchannels that run parallel to the a axis (**Figure 1a**). Alternatively, the structure may be visualized as a result of stacking layers along the b axis. These layers consist of trimers of face-sharing $\text{Ba}_2(\text{O},\text{F})_9\text{--Ba}_3(\text{O},\text{F})_{11}\text{--Ba}_4\text{O}_8$ polyhedra; each trimer is connected to four neighboring trimers belonging to the same layer through Ba_1O_{10} and Ba_5O_{10} polyhedra (**Figure 1b**). Ba_1O_{10} and Ba_5O_{10} polyhedra also link neighboring layers along the b axis. The thermolysis of $\text{Ba}_5(\text{CF}_2\text{BrCOO})_{10}(\text{H}_2\text{O})_7$ in the solid-state was probed using a combination of TGA/DTA and PXRD; results from these analyses are summarized in **Figures 1c** and **1d**. Thermal analysis shows that $\text{Ba}_5(\text{CF}_2\text{BrCOO})_{10}(\text{H}_2\text{O})_7$ decomposes in two stages (**Figure 1c**). The first stage corresponds to an endothermic process in which water molecules are removed. The second one corresponds to the thermolysis of the organic moiety and subsequent crystallization of BaFBr; these processes

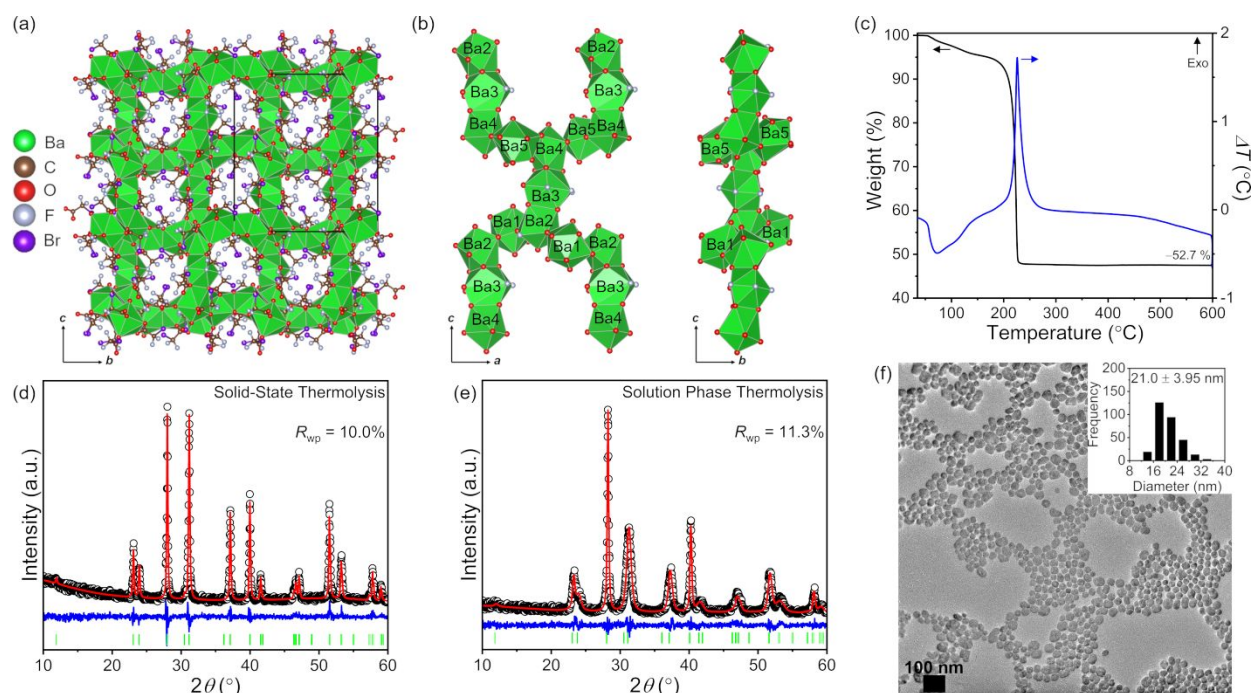


Figure 1. (a) Crystal structure of $\text{Ba}_5(\text{CF}_2\text{BrCOO})_{10}(\text{H}_2\text{O})_7$. Microchannels run in the [100] direction and are lined with $-\text{CF}_2\text{Br}$ groups. Atom splitting in disordered positions has been omitted for clarity; only major occupancy positions are shown. The unit cell is shown with black solid lines. (b) A single layer built of $\text{Ba}(\text{O},\text{F})_n$ polyhedra viewed along [010] and [100] directions. (c) Thermogram and differential thermogram of $\text{Ba}_5(\text{CF}_2\text{BrCOO})_{10}(\text{H}_2\text{O})_7$; the total weight loss is indicated. (d, e) Rietveld analyses of the PXRD patterns of solid-state and solution decomposition products. Experimental (hollow black circles) and calculated patterns (solid red line) are shown along with the difference curve (solid blue line) and tick marks corresponding to BaFBr (vertical green bars). (f) TEM image and size distribution histogram of BaFBr nanocrystals obtained in a mixture of high-boiling point organic solvents.

occur between ≈ 218 and 226 °C and, as expected, are accompanied by an exotherm peaking at 226 °C. The total weight loss (≈ 52.7 wt. %) is in good agreement with the theoretical value computed by assuming quantitative decomposition to BaFBr (53.7 wt. %). Rietveld analysis of the PXRD pattern of the solid obtained after thermal analysis confirms that BaFBr is indeed the only decomposition product (**Figure 1d** and **Table S5**); all diffraction maxima in the pattern can be indexed to tetragonal BaFBr (PDF No. 00–024–0090, $a = 4.5118$ (3) Å, $c = 7.4456$ (5) Å). Motivated by the absence of colloidal routes to BaFBr nanocrystals, we also investigated the thermal decomposition of $\text{Ba}_5(\text{CF}_2\text{BrCOO})_{10}(\text{H}_2\text{O})_7$ in high-boiling point organic solvents; results from these studies are summarized in **Figures 1e** and **1f**. A mixture of oleic acid, 1-octadecene, and trioctylphosphine in a 1:1:1 volume ratio provides good results in terms of phase purity and nanocrystal morphology. Decomposing $\text{Ba}_5(\text{CF}_2\text{BrCOO})_{10}(\text{H}_2\text{O})_7$ at 300 °C in this mixture yields phase pure BaFBr nanocrystals; no diffraction maxima corresponding to secondary crystalline phases are observed in the PXRD pattern (**Figure 1e** and **Table S5**). Electron microscopy reveals that BaFBr nanocrystals exhibit spherical shape with an average diameter of ≈ 21 nm (**Figure 1f**). Outcomes from thermal decomposition studies highlight the utility of $\text{Ba}_5(\text{CF}_2\text{BrCOO})_{10}(\text{H}_2\text{O})_7$ as a dual-halogen precursor to BaFBr, both in the solid-state and in solution. This result along with our previous report on the decomposition of $\text{Ba}_5(\text{CF}_2\text{ClCOO})_{10}(\text{H}_2\text{O})_7$ to BaFCl ¹⁸ demonstrate that, more generally, heterohalocarboxylates provide synthetic access to mixed-halide materials. This family of precursors streamlines synthetic procedures by eliminating the need for external halogenating agents such as corrosive fluorine sources (e.g., F_2 , HF).

$\text{Ba}_5(\text{CF}_2\text{BrCOO})_{10}(\text{H}_2\text{O})_7$ was decomposed in solution in the presence of Yb^{3+} and Er^{3+} to probe the ability to aliovalently dope BaFBr nanocrystals with rare-earths. This experiment also allowed us to explore the feasibility of realizing BaFBr NIR-to-visible upconverting phosphors operating on the basis of Yb^{3+} – Er^{3+} sensitizer–activator pairs. Results from these studies are summarized in **Figure 2** and **Table S6** for the case of BaFBr featuring a 3.0 mol. % nominal total rare-earth concentration; results for other members of the Yb:Er:BaFBr concentration

series are given in the ESI (**Figures S2–S5** and **Table S7**). Rietveld analysis of PXRD data confirms the phase purity of Yb:Er:BaFBr nanocrystals, as no diffraction maxima belonging to crystalline phases other than tetragonal BaFBr are observed (**Figure 2a**). Although nanocrystals appear as ≈ 26 nm cubes at first (**Figure 2b**), closer inspection and quantitative analysis of TEM images reveal that they are not isometric, with an average aspect ratio of ≈ 1.1 . Quantification of metal concentrations via ICP–MS confirms the presence of Yb^{3+} and Er^{3+} (**Figure 2c**). Total rare-earth concentrations increase as a function of their nominal values. Doping efficiencies range between 71 and 87% and experimental ytterbium-to-erbium molar ratios vary between 10 and 18. Attempts to dope BaFBr with a nominal total rare-earth concentration of 7.5% result in the appearance of secondary crystalline phases (see ESI, **Figure S3**). This observation suggests that the experimental solubility limit for codoping Yb^{3+} and Er^{3+} into BaFBr under the experimental conditions described herein is in the order of 4.5–5.0 mol. %. Placing elemental analysis results in the context of our previous studies of rare-earth-doped MFX nanocrystals ($M = \text{Ca}, \text{Sr}, \text{Ba}$; $X = \text{Cl}, \text{Br}$),^{18, 30, 31} we conclude that the solubility of Yb^{3+} – Er^{3+} pairs (Yb:Er molar ratio equal to 9:1) in nanocrystalline MFX (1) increases upon going from calcium to strontium to barium, and (2) increases upon going from fluorobromides to fluorochlorides (see ESI, **Figure S5**). We note that doping trivalent rare-earths must be accompanied by the formation of charge-compensating defects. Pristine and aliovalently doped single crystal and bulk alkaline-earth fluorohalides have been shown to incorporate oxide anions as defects or as charge-compensating species.^{32–35} This may also be the case in Yb:Er:BaFBr nanocrystals, as oxygen traces were certainly present in the reaction medium.

The functionality of Yb:Er:BaFBr nanocrystals as NIR-to-visible upconverters and luminescent thermometers was probed using steady-state spectrofluorometry. Results from these studies are summarized in **Figure 3** for nanocrystals doped with a nominal total rare-earth concentration of 6.0 mol. %. The room-temperature emission spectrum demonstrates the ability to perform NIR-to-visible light upconversion (**Figure 3a**). Bands at 525, 545, and 660 nm are observed upon 980 nm excitation, corresponding to the $^4\text{F}_{9/2} \rightarrow ^4\text{I}_{15/2}$, $^2\text{H}_{11/2} \rightarrow ^4\text{I}_{15/2}$, and

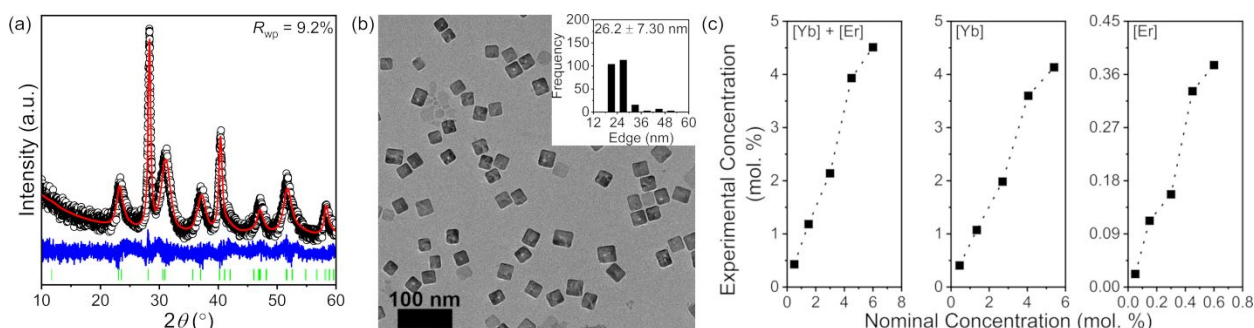


Figure 2. (a) Rietveld analysis of the PXRD pattern of Yb:Er:BaFBr nanocrystals doped with a nominal rare-earth concentration of 3.0 mol. %. Experimental (hollow black circles) and calculated patterns (solid red line) are shown along with the difference curve (solid blue line) and tick marks corresponding to BaFBr (vertical green bars). (b) Corresponding TEM image and size distribution histogram. Nanocrystal size distribution is obtained by estimating edge length as $(\text{width} \times \text{length})^{1/2}$ (see text for details). (c) Metal concentration curves for the Yb:Er:BaFBr concentration series. Dotted lines are guides-to-the-eye.

$^4S_{3/2} \rightarrow ^4I_{15/2}$ transitions of the Er^{3+} activator, respectively. Additionally, a very weak band arising from the $^2H_{9/2} \rightarrow ^4I_{15/2}$ transition is observed at ≈ 410 nm. To the best of our knowledge, this is the first report of ytterbium-sensitized upconversion in BaFBr. Since the spectrum is dominated by the band centered at 660 nm, Yb:Er:BaFBr behave as red phosphors under NIR excitation. Red and red-orange upconverting phosphors have also been obtained using SrFCl as a host.^{30, 36} The spectral distribution of the upconverted emission does not change significantly with the rare-earth concentration; integrated intensities, on the other hand, increase with doping (see ESI, **Figures S6** and **S7**). 6.0 mol. % Yb:Er:BaFBr nanocrystals were thus used to test their ability to operate as ratiometric luminescent thermometers. To this end, the temperature-dependence of the emissions from the $^2H_{11/2}$ and $^4S_{3/2}$ thermally coupled levels of Er^{3+} was monitored between 150 and 450 K. Inspection of emission spectra shows that the intensity of the 525 nm band increases with temperature, whereas that of the 545 nm band decreases (**Figure 3b**). The luminescence intensity ratio ($R(T)$) between these two bands was fit using equation (1)

$$R(T) = \frac{I(^2H_{11/2} \rightarrow ^4I_{15/2})}{I(^4S_{3/2} \rightarrow ^4I_{15/2})} = A \exp\left(-\frac{B}{T}\right) + C \quad (1)$$

$$S_R(T) = \frac{1}{R(T)} \frac{dR(T)}{dT} \quad (2)$$

and relative thermometric sensitivity ($S_R(T)$) was computed using equation (2). Intensities were extracted by integrating green emission bands between 505 and 535 nm ($I(^2H_{11/2} \rightarrow ^4I_{15/2})$) and between 535 and 570 nm ($I(^4S_{3/2} \rightarrow ^4I_{15/2})$). $R(T)$ is adequately fit using $A = 7.6$ (6), $B = 1106$ (35) K, and $C = 0.011$ (6) as adjustable parameters (**Figure 3c**). Sensitivity reaches a maximum of $2.1 \times 10^{-2} \text{ K}^{-1}$ at 200 K and decreases to $1.1 \times 10^{-2} \text{ K}^{-1}$ at room-temperature. These values are in line with those obtained for upconverting luminescent thermometers based on other alkaline-earth fluorohalide hosts such as CaFCl ($2.2 \times 10^{-2} \text{ K}^{-1}$ at 200 K; $1.0 \times 10^{-2} \text{ K}^{-1}$ at 300 K),³¹ SrFCl ($1.7 \times 10^{-2} \text{ K}^{-1}$ at 200 K; $\approx 1.0 \times 10^{-2} \text{ K}^{-1}$ at 300 K),³⁷ and SrFBr ($2.1 \times 10^{-2} \text{ K}^{-1}$ at 200 K; $1.2 \times 10^{-2} \text{ K}^{-1}$ at 300 K).³⁷ Their similarity simply reflects the rather restricted range of sensitivities that may be achieved in single-activator ratiometric thermometers based on thermally coupled emissions. Finally, the thermometric performance of Yb:Er:BaFBr nanocrystals was further evaluated by computing repeatability, mean calculated temperature ($\langle T_{\text{calculated}} \rangle$), and temperature resolution (ΔT) at 175, 300, and 400 K. Nanocrystals were subject to 10 heating-cooling cycles (**Figure 3d**). Repeatability was calculated using equation (3), where $R_i(T)$ is the value of the intensity ratio in the i th cycle and $\langle R(T) \rangle$ is the average value computed over 10 cycles.

$$\text{Repeatability}(T) = 100 \times \left[1 - \frac{\max |R_i(T) - \langle R(T) \rangle|}{\langle R(T) \rangle} \right] \quad (3)$$

For each cycle, temperatures were backcalculated using equation (1) and the average and standard deviation of these

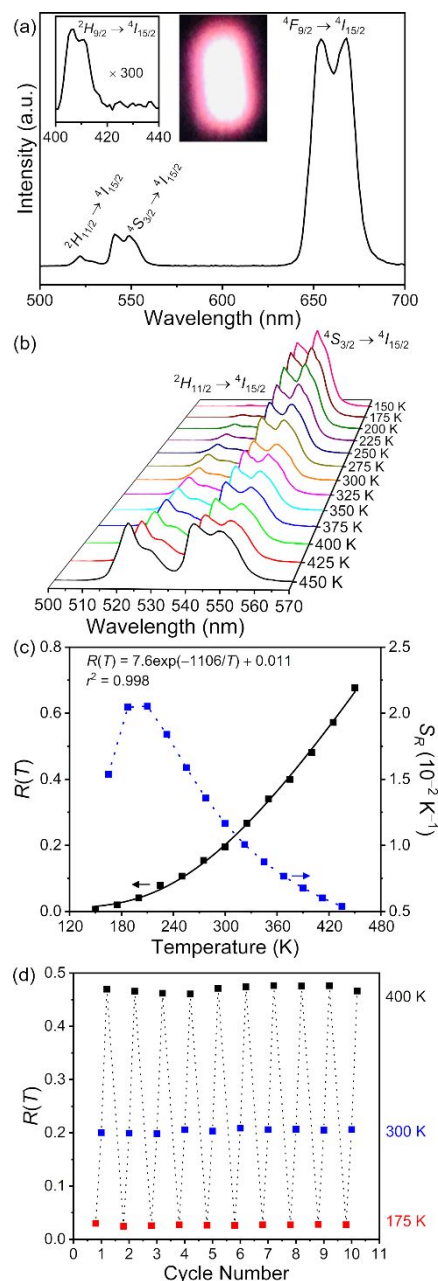


Figure 3. Room temperature (a) and variable temperature (b) emission spectra of Yb:Er:BaFBr nanocrystals doped with a nominal total rare-earth concentration of 6.0 mol. % under 980 nm excitation. Insets in (a) show the room temperature emission spectrum in the blue region and a digital picture of the sample under NIR illumination. (c) Luminescence intensity ratio ($R(T)$) and relative thermometric sensitivity ($S_R(T)$) as a function of temperature. Fit of equation (1) to experimental ratios is depicted with a solid line. (d) Cyclability plot; dotted lines are guides-to-the-eye.

distributions were used to estimate temperature accuracy and resolution (see ESI, **Table S8**). Repeatabilities of 89, 99, and 99% are thus estimated at 175, 300, and 400 K, respectively. Likewise, mean calculated temperatures equal to 180.2 (2.6), 300.9 (1.5), and 393.5 (1.8) K are obtained.

Conclusions

The utility of $\text{Ba}_5(\text{CF}_2\text{BrCOO})_{10}(\text{H}_2\text{O})_7$ as a precursor to BaFBr was demonstrated. Thermolysis of this organic–inorganic hybrid in the solid-state and in solution yielded crystalline, phase-pure BaFBr at 300 °C. The organic moiety CF_2BrCOO acted as an in situ fluorinating and brominating agent. Pristine and doped BaFBr nanocrystals were obtained upon decomposition of the precursor in a mixture of high-boiling point organic solvents. Yb:Er:BaFBr nanocrystals were shown to serve as upconverting phosphors whose temperature-dependent green emission renders them ratiometric thermometers between 150 and 450 K. Results presented in this article further support heterohalogenated monocarboxylates as a family of hybrid precursors broadly applicable to the synthesis of mixed-halide materials. From the perspective of realizing solution-processable photostimulable phosphors, future synthetic efforts should seek to (1) develop the chemistry presented herein to dope divalent lanthanides such as Eu^{2+} into BaFBr nanocrystals, and (2) functionalize the nanocrystals' surface.

Conflicts of interest

There are no conflicts to declare.

Acknowledgements

This work was supported by the National Science Foundation (DMR–2003118). The authors are also grateful for the support of the Department of Chemistry at Wayne State University and for the use of the X-ray and Electron Microscopy cores in the Lumigen Instrument Center (National Science Foundation, MRI–1427926, –0216084, and –2018587).

Notes and references

- Sonoda, M.; Takano, M.; Miyahara, J.; Kato, H., Computed Radiography Utilizing Scanning Laser Stimulated Luminescence. *Radiology* 1983, **148**, 833–838.
- Takahashi, K.; Kohda, K.; Miyahara, J.; Kanemitsu, Y.; Amitani, K.; Shionoya, S., Mechanism of Photostimulated Luminescence in BaFX:Eu^{2+} ($X = \text{Cl, Br}$) Phosphors. *J. Lumin.* 1984, **31–32**, 266–268.
- Takahashi, K.; Miyahara, J.; Shibahara, Y., Photostimulated Luminescence (PSL) and Color Centers in BaFX:Eu^{2+} ($X = \text{Cl, Br, I}$) Phosphors. *J. Electrochem. Soc.* 1985, **132**, 1492–1494.
- Klee, R. J., An X-ray Diffraction Study of $(\text{Ba,Sr})\text{F}_{1+x}\text{Br}_{1-x}:\text{Eu}^{2+}$, A New X-ray Image Receptor Material. *J. Phys. D: Appl. Phys.* 1995, **28**, 2529–2533.
- Schlapp, M.; Bulur, E.; von Seggern, H., Photo-Stimulated Luminescence of Calcium Codoped BaFBr:Eu^{2+} X-ray Storage Phosphors. *J. Phys. D: Appl. Phys.* 2002, **36**, 103–108.
- Wang, X.; Riesen, H.; Stevens-Kalceff, M. A.; Rajan, R. P., Room Temperature Hole-Burning of X-ray Induced Sm^{2+} in Nanocrystalline $\text{Ba}_{0.5}\text{Sr}_{0.5}\text{FCl}_{0.5}\text{Br}_{0.5}:\text{Sm}^{3+}$ Prepared by Mechanochemistry. *J. Phys. Chem. A* 2014, **118**, 9445–9450.
- Zhao, W.; Mi, Y.; Su, M.; Song, Z.; Xia, Z., Response Time of Photostimulated Luminescence of BaFX:Eu^{2+} and BaFCl:Pr^{3+} Under Near-Infrared Light Stimulation. *J. Electrochem. Soc.* 1996, **143**, 2346–2348.
- Zhang, J.; Riesen, N.; Kasim, L. T.; Badek, K.; Riesen, H., Mechanochemical Preparation of Nanocrystalline Metal Halide Phosphors. *J. Mater. Sci.* 2018, **53**, 13643–13659.
- Zimmermann, J.; Kolb, R.; Hesse, S.; Schlapp, M.; Schmechel, R.; Seggern, H. v., Preparation-Induced F-Centre Transformation in BaFBr:Eu^{2+} . *J. Phys. D: Appl. Phys.* 2004, **37**, 2352–2357.
- von Seggern, H.; Hesse, S.; Zimmermann, J.; Appleby, G. A.; Meng, X.; Fasel, C.; Riedel, R., New Synthesis of High-Quality Storage Phosphors. *Radiat. Meas.* 2010, **45**, 478–484.
- Leblans, P.; Vandembroucke, D.; Willems, P., Storage Phosphors for Medical Imaging. *Materials* 2011, **4**, 1034–1086.
- Meng, X.-G.; Wang, Y.-S.; He, D.-W., Synthesis and Optical Properties of BaFBr and BaFBr:Eu^{2+} Nanoparticles. *J. Nanosci. Nanotechnol.* 2010, **10**, 2190–2192.
- Liang, Q.; Shi, Y.; Ma, W.; Li, Z.; Yang, X., Uniform Square-Like BaFBr:Eu^{2+} Microplates: Controlled Synthesis and Photoluminescence Properties. *RSC Adv.* 2012, **2**, 5403–5410.
- Liang, Q.; Li, Z.; Ma, W.; Shi, Y.; Yang, X., Controlled Synthesis and Optical Properties of BaFBr:Eu^{2+} Crystals via Ethanol/Water Solutions. *Mater. Res. Bull.* 2012, **47**, 2357–2363.
- Chen, L.; Wu, Y.; Huo, H.; Tang, B.; Fu, Y.; Hu, X.; Sun, C.; Zhou, S., Study on the Fluorescence Properties of Micron-Submicron-Nano BaFBr:Eu^{2+} Phosphors. *New J. Chem.* 2020, **44**, 13118–13124.
- Wang, X.; Riesen, H., Mechanochemical Synthesis of an Efficient Nanocrystalline BaFBr:Eu^{2+} X-ray Storage Phosphor. *RSC Adv.* 2015, **5**, 85506–85510.
- Olchowka, J.; Hagemann, H.; Delgado, T.; Wickleder, C., The Influence of Ionothermal Synthesis Using BmimBF_4 as a Solvent on Nanophosphor BaFBr:Eu^{2+} Photoluminescence. *Nanoscale* 2018, **10**, 19706–19710.
- Dissanayake, K. T.; Amarasinghe, D. K.; Suescun, L.; Rabuffetti, F. A., Accessing Mixed-Halide Upconverters Using Heterohaloacetate Precursors. *Chem. Mater.* 2019, **31**, 6262–6267.
- Krause, L.; Herbst-Irmer, R.; Sheldrick, G. M.; Stalke, D., Comparison of Silver and Molybdenum Microfocus X-ray Sources for Single-Crystal Structure Determination. *J. Appl. Crystallogr.* 2015, **48**, 3–10.
- Sheldrick, G., Crystal Structure Refinement with SHELXL. *Acta Crystallogr. C* 2015, **71**, 3–8.
- Sheldrick, G. M. *SHELXL 2014/7: Program for Crystal Structure Solution*, University of Gottingen: 2014.
- Hubschle, C. B.; Sheldrick, G. M.; Dittrich, B., ShelXle: a Qt Graphical User Interface for SHELXL. *J. Appl. Crystallogr.* 2011, **44**, 1281–1284.
- Momma, K.; Izumi, F., VESTA 3 for Three-Dimensional Visualization of Crystal, Volumetric and Morphology Data. *J. Appl. Crystallogr.* 2011, **44**, 1272–1276.
- Rietveld, H. M., Line Profiles of Neutron Powder-Diffraction Peaks for Structure Refinement. *Acta Crystallogr.* 1967, **22**, 151–152.
- Rietveld, H. M., A Profile Refinement Method for Nuclear and Magnetic Structures. *J. Appl. Crystallogr.* 1969, **2**, 65–71.
- Larson, A. C.; Von Dreele, R. B. *General Structure Analysis System (GSAS)*; Los Alamos National Laboratory: 2000.
- Toby, B. H., EXPGUI, a Graphical User Interface for GSAS. *J. Appl. Crystallogr.* 2001, **34**, 210–213.
- Thompson, P.; Cox, D. E.; Hastings, J. B., Rietveld Refinement of Debye–Scherrer Synchrotron X-ray Data from Al_2O_3 . *J. Appl. Crystallogr.* 1987, **20**, 79–83.
- Cheetham, A. K.; Rao, C. N. R.; Feller, R. K., Structural Diversity and Chemical Trends in Hybrid Inorganic–Organic Framework Materials. *Chem. Commun.* 2006, **0**, 4780–4795.

- 30 Dissanayake, K. T.; Rabuffetti, F. A., Multicolor Emission in Chemically and Structurally Tunable Er:Yb:SrFX (X = Cl, Br) Upconverting Nanocrystals. *Chem. Mater.* 2018, **30**, 2453–2462.
- 31 Dhanapala, B. D.; Munasinghe, H. N.; Rabuffetti, F. A., Temperature-Dependent Luminescence of CaFCl:Yb,Er Upconverting Nanocrystals. *J. Lumin.* 2021, **235**, 117974.
- 32 Catlow, C.R.A., Oxygen Incorporation in the Alkaline-Earth Fluorohalides. *J. Phys. Chem. Solid.* 1977, **38**, 1131–1136.
- 33 Radzhabov, E.; Otroshok, V., Optical Spectra of Oxygen Defects in BaFCl and BaFBr Crystals. *J. Phys. Chem. Solid.* 1995, **56**, 1–7.
- 34 Chen, X.Y.; Zhao, W.; Cook, R.E.; Liu, G.K., Anomalous Luminescence Dynamics of Eu³⁺ in BaFCl Microcrystals. *Phys. Rev. B* 2004, **70**, 205122.
- 35 Ju, Q.; Liu, Y.S.; Li, R.F.; Liu, L.Q.; Luo, W.Q.; Chen, X.Y. Optical Spectroscopy of Eu³⁺-Doped BaFCl Nanocrystals. *J. Phys. Chem. C* 2009, **113**, 2309–2315.
- 36 Zhang, J.; Riesen, N.; Riesen, H., Mechanochemically Prepared SrFCl Nanophosphor Co-Doped with Yb³⁺ and Er³⁺ for Detecting Ionizing Radiation by Upconversion Luminescence. *Nanoscale* 2017, **9**, 15958–15966.
- 37 Perera, S. S.; Dissanayake, K. T.; Rabuffetti, F. A., Alkaline-Earth Fluorohalide Nanocrystals for Upconversion Thermometry. *J. Lumin.* 2019, **207**, 416–423.